T. Ebbers[1]
e-mail: Tino.Ebbers@imv.liu.se

L. Wigström

Department of Medicine and Care,
Clinical Physiology and
Department of Biomedical Engineering,
Linköping University,
SE-581 85 Linköping, Sweden

A. F. Bolger
Department of Medicine,
University of California,
San Francisco, CA

B. Wranne
Department of Medicine and Care,
Clinical Physiology,
Linköping University,
SE-581 85 Linköping, Sweden

M. Karlsson
Department of Biomedical Engineering,
Linköping University,
SE-581 85 Linköping, Sweden

Noninvasive Measurement of Time-Varying Three-Dimensional Relative Pressure Fields Within the Human Heart

Understanding cardiac blood flow patterns is important in the assessment of cardiovascular function. Three-dimensional flow and relative pressure fields within the human left ventricle are demonstrated by combining velocity measurements with computational fluid mechanics methods. The velocity field throughout the left atrium and ventricle of a normal human heart is measured using time-resolved three-dimensional phase-contrast MRI. Subsequently, the time-resolved three-dimensional relative pressure is calculated from this velocity field using the pressure Poisson equation. Noninvasive simultaneous assessment of cardiac pressure and flow phenomena is an important new tool for studying cardiac fluid dynamics. [DOI: 10.1115/1.1468866]

Introduction

Understanding cardiac blood flow patterns is important in the clinical assessment of cardiovascular function, as well as in the design of valve prostheses and valvular surgery. Established methods for measuring the function of the heart muscle can be extended by understanding the cardiac flow field and the pressure differences that are its driving force in healthy as well as diseased hearts.

Computational methods allow investigation of the effects of individual parameters on a system. Simulations have proven very useful as study, teaching, and research aids. Lumped parameter models have increased our knowledge and understanding of cardiac function and the interaction between the left atrium, the left ventricle, and the mitral valve in particular [1]. Increasing computer power and improved computational fluid dynamics (CFD) algorithms allow increasingly detailed models that can provide explicit information about the relevant flow fields. These simulations become more realistic as increasing amounts of physiological information are incorporated. A three-dimensional model of the left ventricle, based on a cast of a dog heart, has been used to simulate the flow patterns in the left ventricle [2]. By including the myocardium in the simulation, the interaction between blood and cardiac structures can be obtained, resulting in more physiologically correct motion of the heart muscle. Peskin et al., accomplished this by allowing the fluid and structure to be defined on separate grids [3]. Although these simulations can provide information about the flow field, the physiological validity of the results remains uncertain, as the simulations are based on assumptions about the heart's geometry and functioning.

Noninvasive three-dimensional measurement of cardiac velocity fields allows detailed investigation of flow patterns in the large heart chambers of individuals. Phase-contrast magnetic resonance imaging (MRI) has been shown to produce accurate measurement of the velocity vector [4–6]. Investigation of flow patterns using two-dimensional vector plots has confirmed vortical flow patterns in the left ventricle during diastole predicted by simulations and model studies [7]. Three-dimensional particle trace visualization has revealed different inflow pathways during early and late diastole [8] and vortical flow in the left atrium during mid-diastole and systole [9]. Cardiac pressure differences can be calculated along these particle traces, or other user-defined lines [10]. A method has been presented for the calculation of the relative cardiac pressure field from a measured velocity field, based on the Navier-Stokes equation [11]. The quality of the pressure field in that study was limited by the accuracy of the cardiac velocity field, which was estimated from a sequence of CT cardiac images. The method has, however, successfully been used and validated in the aorta for obtaining the relative aortic pressure field from time-resolved phase-contrast MRI velocity data [12,13].

Here, detailed information about the pressure and flow phenomena in the left side of the heart is yielded, by combining noninvasive velocity measurements with computational fluid mechanics. The velocity field throughout the left atrium and left ventricle of a normal human heart is measured using time-resolved three-dimensional phase-contrast MRI. The three-dimensional relative pressure in each time frame is then calculated from this velocity field using the pressure Poisson equation.

Methods

Velocity Measurement. The time-resolved three-dimensional velocity vector field of a human heart (a 53 year old healthy female volunteer, heart rate: 63 bpm) with sufficient resolution and signal-to-noise ratio to describe the spatial and temporal characteristics of intracardiac flow was obtained by use of a novel

[1]Author to whom correspondence should be addressed.

Contributed by the Bioengineering Division for publication in the JOURNAL OF BIOMECHANICAL ENGINEERING. Manuscript received by the Bioengineering Division August 16, 2001; revised manuscript received January 24, 2002. Associate Editor: A. P. Yoganathan.

time-resolved three-dimensional phase contrast MRI pulse sequence [14,15]. Data were obtained using a 1.5 T Signa Horizon Echospeed scanner (General Electric Medical Systems, Milwaukee, WI). A $34.0\times34.0\times11.2$ cm axial three-dimensional volume with a spatial resolution of $1.4\times4.0\times4.0$ mm was imaged, using TR=18 ms, TE=7.2 ms, and VENC=0.6 m/s. Velocity encoded data were acquired in all three directions at 16 times for each phase-encoding step, with a sampling interval of 72 ms. A complete set of *k*-space data was interpolated in the time domain for 32 time frames using an interpolation method based on a normalized convolution algorithm with a Gaussian interpolation function [14,16]. In order to reduce the acquisition time to 18 minutes, only a cylindrical region of *k*-space was collected by excluding the corners of the k_y-k_z plane [17] combined with a reduced-field -of-view method [18]. After zero-filling to a size of $256\times256\times32$ and three-dimensional inverse Fourier transformation, the data were corrected for phase contribution of concomitant field effects [19] and eddy current effects [20].

The Pressure Poisson Equation. The relationship between the pressure gradients $\nabla p=(\partial p/\partial x,\partial p/\partial y,\partial p/\partial z)$ and velocities $\mathbf{V}=(u,v,w)$ in an incompressible, laminar, Newtonian fluid with density ρ and viscosity μ is expressed by the Navier-Stokes equations, describing the conservation of momentum [21]

$$\nabla p=-\rho\frac{\partial\mathbf{V}}{\partial t}-\rho\mathbf{V}\cdot\nabla\mathbf{V}+\mu\nabla^2\mathbf{V}+\mathbf{F} \tag{1}$$

where the first term on the right-hand side results from the transient inertia and the second term from the convective inertia. The third term describes the viscous resistance and the variable **F** represents the body forces. For a closed system, the body forces have no effect on the flow, as the buoyancy force cancels out the gravitation force. The Navier-Stokes equations can be solved in combination with the continuity equation, describing the conservation of mass [21]

$$\nabla\cdot\mathbf{V}=0 \tag{2}$$

given an initial condition and boundary conditions.

In this study we have measured the velocity field, and hence the pressure gradient field can be obtained directly from the velocity field using Eq. (1). In principle, integration of the pressure gradient field derives the relative pressure field. However, the result will be dependent on the integration path, mainly due to noise which is present in the velocity data. The method generally used to obtain the pressure field from a velocity field is to take the divergence of Eq. (1), which derives a Poisson equation, called the Pressure Poisson Equation (PPE) [22]

$$\nabla^2 p=\nabla\cdot\mathbf{b} \tag{3}$$

where **b** denotes the pressure gradient field obtained from Eq. (1) while dropping the body force term. Using this equation, the pressure field can be obtained from the velocity field up to an integration constant, that is different for each time frame, which makes the pressure field relative. Equation (3) can also be obtained by a least square formulation, where a pressure field p is sought that has a pressure gradient field ∇p that is a least square solution of the pressure gradient field **b** obtained from Eq. (1), as shown by Song et al. [11].

To be able to solve the PPE, boundary conditions are necessary. It has been shown that the Neumann boundary condition is appropriate for the PPE [23]. The Neumann boundary condition emerges by applying the PPE at the boundaries of the flow $\partial\Omega$ and projecting it onto the unit normal vector $\hat{\mathbf{n}}$ as

$$\nabla p\cdot\hat{\mathbf{n}}=\mathbf{b}\cdot\hat{\mathbf{n}}. \tag{4}$$

A semi-automatic delineation of the left ventricular blood pool was used to set these boundary conditions, utilizing magnitude image as well as velocity data. The segmentation included the left atrium during diastole, but excluded it during systole when the mitral valve is closed.

Numerical Implementation. A numerical solution to solve the PPE for an irregular volume is troublesome. The segmented region is therefore extended to a rectangular computational domain Ω, on which the boundary conditions can easily be implemented. The pressure gradient field **b** outside the fluid volume Ω_F is iteratively updated to ∇p, as described by Song et al. [11]

$$\begin{aligned}\nabla^2 p^{(m)}&=\nabla\cdot\mathbf{b}^{(m)} \qquad \text{within } \Omega\\ \nabla p^{(m)}\cdot\hat{\mathbf{n}}&=\mathbf{b}^{(m)}\cdot\hat{\mathbf{n}} \qquad \text{at } \partial\Omega\end{aligned} \tag{5}$$

where

$$\mathbf{b}^{(m+1)}=\begin{cases}\mathbf{b} & \text{within } \Omega_F\\ \nabla p^{(m)} & \text{at } \Omega-\Omega_F\end{cases} \tag{6}$$

m and $m+1$ are two successive iteration steps.

The pressure gradient was calculated using a second-order central-difference discretization of Eq. (1) [24], after the velocity field had been resampled to a resolution of $2.0\times2.0\times2.0$ mm using linear interpolation. The viscosity of blood was set to 0.004 $\mathrm{Ns/m^2}$ and the density to 1060 $\mathrm{kg/m^3}$.

The PPE was solved using an iterative method, which is designated for systems of large size. Using a second-order central difference for the gradient calculation directly derives the Jacobi iteration method in explicit form [25]. Starting at an initial condition, here set to zero, the pressure $p_{i,j,k}$ in a voxel (i, j, k) is replaced for every iteration by a weighted average of its nearest neighbors and **b** according to

$$\begin{aligned}p_{i,j,k}^{(m+1)}=\frac{1}{6}(&p_{i-1,j,k}^{(m)}+p_{i+1,j,k}^{(m)}+p_{i,j-1,k}^{(m)}+p_{i,j+1,k}^{(m)}+p_{i,j,k-1}^{(m)}\\&+p_{i,j,k+1}^{(m)}-d^2\nabla\cdot\mathbf{b}_{i,j,k}^{(m+1)})\end{aligned} \tag{7}$$

where d is the spatial resolution, here 2.0 mm. This process continues until a convergence condition is fulfilled, here defined as

$$R=\frac{|p^{(m+1)}-p^{(m)}|}{\nabla^2 p^{(m+1)}}. \tag{8}$$

Convergence was assumed at $R<1\cdot10^{-10}$.

Visualization. Both the measured velocity field and the calculated relative pressure field were imported into the visualization software Ensight (CEI Inc., Research Triangle Park, NC, USA). The three-dimensional relative pressure field, a scalar field, was visualized using cut planes color-coded by pressure. The velocity field, a vector field, could be visualized using either color coding or particle trace visualization [14]. A particle trace can be either a streamline or a pathline. A pathline is the calculated trajectory that a fluid follows as it moves through space over time and is a powerful tool for intuitive time-resolved animation of the velocity field. A velocity field at a given instant, as in a time frame, is often best visualized by a streamline, which is a line tangent to the velocity vector field at every point. The interaction between the velocity and the relative pressure field was studied mainly by visualizing the velocity field using streamlines emitted backwards and forwards starting from the pressure color-coded cut planes.

To further facilitate the study of transmitral and intraventricular pressure gradients over the cardiac cycle, the pressure differences

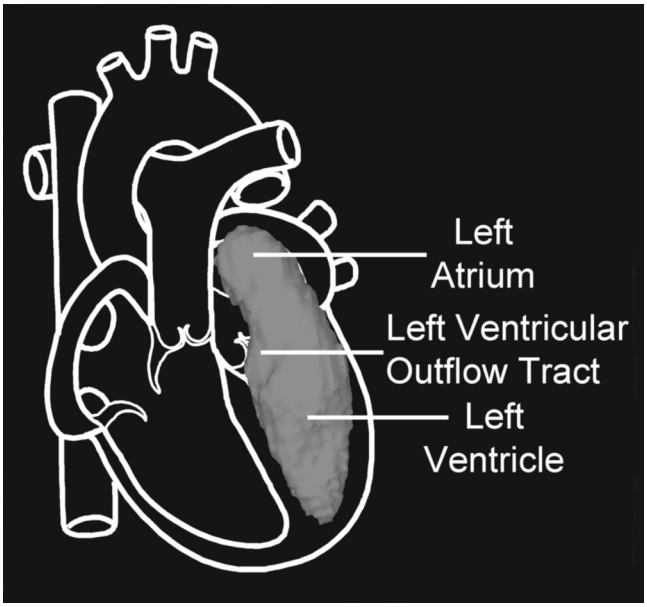

Fig. 1 Schematic drawing showing the orientation of the segmented three-dimensional volume containing the left atrium and ventricle during diastole

between several representative points in the left side of the heart were plotted over time. Points were defined in the left atrium, at the base of the ventricle near the mitral valve, and in the left ventricular outflow tract (LVOT). These were subtracted from the relative pressure at the left ventricular apex, which was defined within each frame as the point on the segmentation contour at greatest distance from the left atrial point. The differences in relative pressure between these points were plotted over the cardiac cycle.

Results

The relative pressure field was calculated from the velocity field using the delineation of the left atrium and ventricle (Figs. 1 and 2), and was visualized using color-coded cut planes, oriented in the long and short axes of the heart. The velocity field was visualized using streamlines generated from these planes.

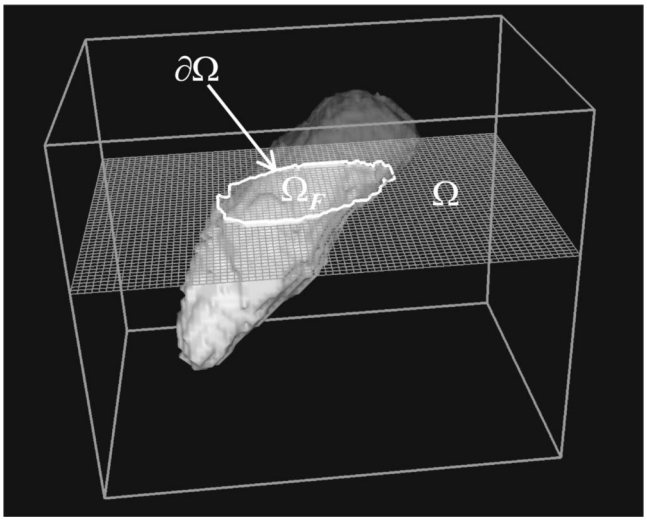

Fig. 2 The computational domain Ω containing the segmented three-dimensional fluid volume Ω_F with boundary $\partial\Omega$

At the onset of early diastolic inflow, a pressure gradient can be seen throughout the left atrium and ventricle. The pressure differences, initiated by relaxation and deformation of the left ventricle, accelerate the blood from the left atrium to the left ventricle (Fig. 3(*a*)). Once initiated, inflow rapidly reduces the transmitral pressure difference (Fig. 3(*b*)). Continuing inflow, caused by inertia, creates a reversal of the initial transmitral pressure difference (Fig. 3(*c*)). This results in deceleration and redirection of blood flow, with subsequent decline and extinction of the reversed pressure gradient. A similar evolution, with lower amplitude of the pressure differences, can also be observed during late diastole (Figs. 3(*d–f*)).

During the peak phases of early and late diastole, the transmitral pressure gradients are small and vortices can be seen around the mitral inflow (Figs. 3(*b*) and 3(*e*)). These vortices dominate the relative pressure field on the ventricular side of the mitral valve, with pressure minimums in the centers of the vortices, as shown in Fig. 4.

At the onset of systole, a pressure gradient arises caused by contraction and reshaping of the left ventricle (Fig. 3(*g*)). This pressure field redirects and accelerates the blood, which still flows in a vortical pattern, towards the left ventricular outflow tract. Once initiated, outflow rapidly reduces the pressure gradients (Fig. 3(*h*)), resulting in a pressure gradient reversal at the end of systole (Fig. 3(*i*)).

The velocity at the base and the transmitral and intraventricular pressure differences over time are shown in Fig. 5. Early and late diastolic inflow can be recognized from the velocity at the base of the ventricle. The pressure differences demonstrate the reversal of the transmitral pressure gradient during left ventricular filling and ejection. During these phases, intraventricular pressure gradients can also be observed.

Discussion

Three-dimensional flow and relative pressure fields in the human left ventricle can be obtained by calculations based on noninvasive MRI velocity measurements. Simultaneous assessment of pressure and flow phenomena in the left atrium and ventricle throughout the cardiac cycle allows an intuitive demonstration of the important flow and pressure events that characterize cardiac fluid dynamics.

We found a similar pattern of transvalvular pressure differences during both ventricular filling and ejection. This pattern starts with relaxation or contraction of one of the large blood chambers, which creates a transvalvular pressure difference and initiates acceleration of blood. Once initiated, the blood flow rapidly reduces the transvalvular pressure difference. Continuing inflow, caused by inertia, creates a reversal of the initial transvalvular pressure difference, which results in deceleration and redirection of blood flow. The existence of this transvalvular pressure difference reversion for left ventricular filling and ejection is well known from studies using pressure transducer pairs [26,27].

In addition to transvalvular pressure differences, pressure differences within the left atrium and ventricle chambers themselves could be seen. Intraventricular pressure gradients have been reported from previous experimental animal studies using pressure transducer pairs. Our intraventricular pressure findings are in agreement with these catheter-based animal studies [28–32], but give a much more complete spatial description of the pressure differences and apply to the healthy human heart. These pressure gradients are expected to change in the setting of cardiac dysfunction, such as with acute myocardial ischemia [30], raising the possibility of demonstrating these clinically relevant pressure effects with this method.

Pressure differences caused by transient inertia, which is due to changes in the flow environment such as relaxation or contraction of the ventricle, predominate at the onset and termination of both ventricular filling and ejection and result in movement of the

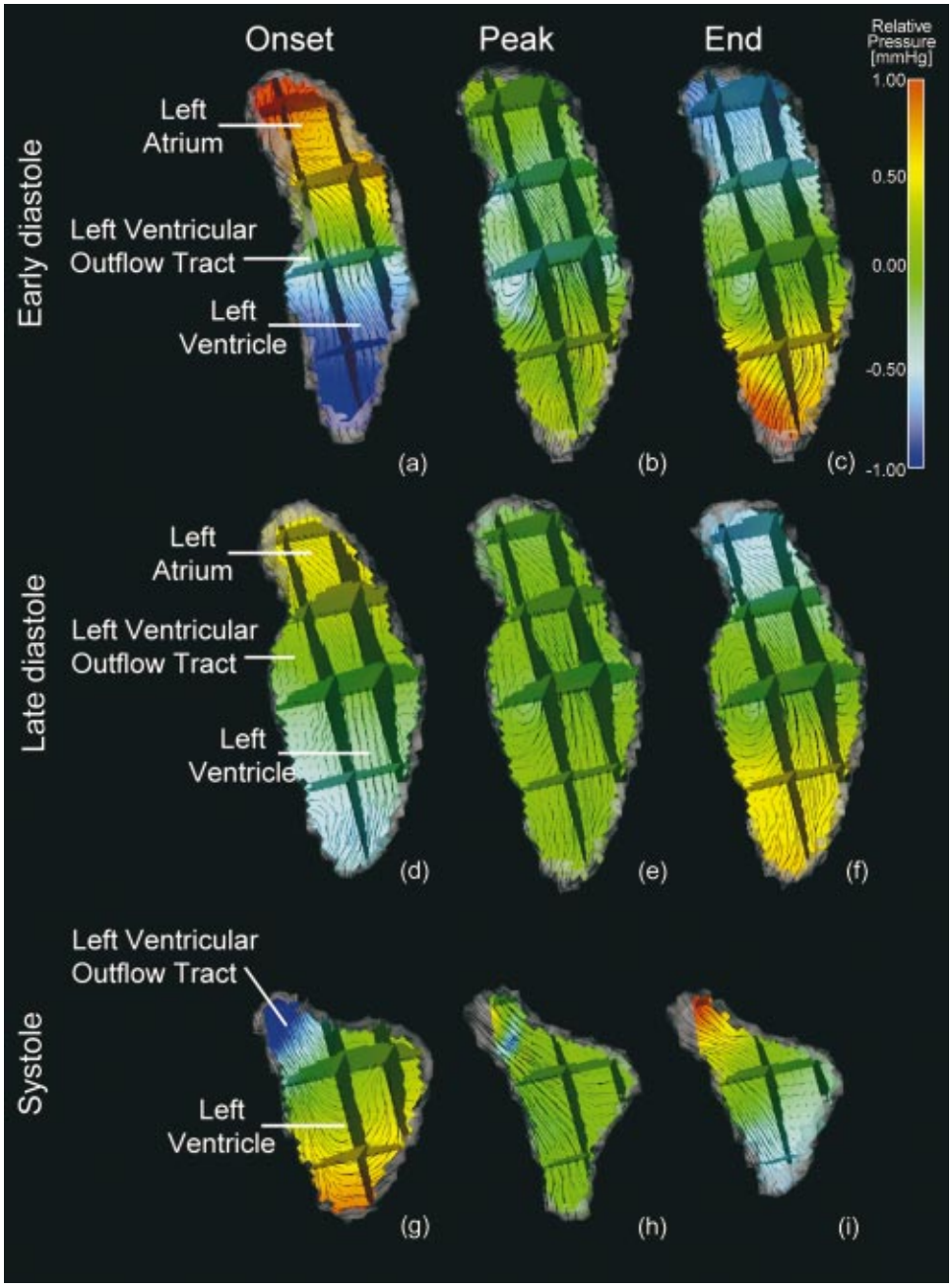

Fig. 3 A long axis slice of the relative pressure field (color) and the velocity field (black streamlines) in the left side of the normal human heart at the onset, peak, and end of the early phase of diastolic inflow (*a*)–(*c*), the late phase of diastolic inflow (*d*)–(*f*), and ventricular systole (*g*)–(*i*).

blood. These are small at the peak of early and late diastolic inflow, however. During these phases the pressure differences are principally due to convective inertia. These pressure differences are a consequence of the flow field itself and do not contribute to blood movement. This effect is demonstrated by the observed vortices that surround the ventricular inflow during the peak early and late diastolic phases. The vortices' pressure fields balance their minimum pressures at the vortex core against the centrifugal forces at the periphery. These pressure differences across the vortices dominate the overall pressure field around the mitral valve during peak inflow phases. The location, shape, and size of the vortices suggest that they are closely related to the ventricular side of the anterior and posterior mitral leaflets. While they do not contribute to global blood movement, these regional pressure differences may be important to other critical aspects of the cardiac cycle: *in-vitro* experiments suggest that the pressure fields of these left ventricular vortices may assist in the subsequent closure of the mitral valve [33]. Other studies question the role of these vortices on valve closure, instead attributing valve closure mainly to the large adverse pressure gradient during inflow deceleration [34] or to the effects of tension in the chordae tendinae [35]. The small pressure differences across the mitral valve found in this study suggest that an equilibrium exists between the reversed pressure gradient, the chordal tension and the mitral inflow, and that this may be changed by small changes in the flow pattern, such as a vortical flow.

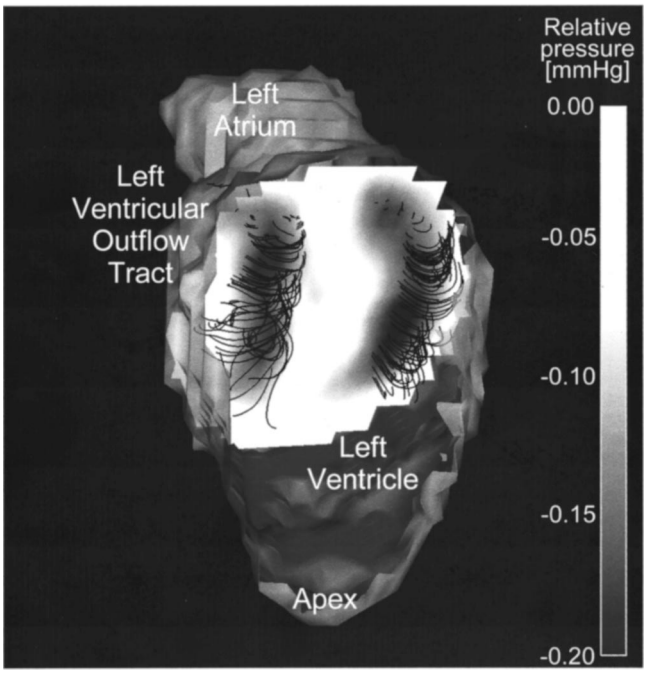

Fig. 4 The relative pressure field (gray scale) and the velocity field (black streamlines) around the mitral valve at the peak of the late phase of diastolic inflow. A single short axis slice of the three-dimensional data set is shown.

We used a semi-automatic segmentation of the blood pool based on the velocity as well as the magnitude data. This segmentation is both very time consuming and difficult to perform at all time points in the cardiac cycle. Using three-dimensional MRI, the inflow of nonsaturated blood is small during some cardiac phases, and this decreases the contrast between myocardium and blood. At the same time, the velocities of the blood pool and the myocardium are of the same order of magnitude. Delineation of the myocardial-blood interface using particle traces [36] may allow automatic myocardial segmentation, with improvements in time savings as well as accuracy.

The accuracy of the pressure calculation is dependent upon the quality of the velocity data. Respiratory motion results in some spatial smoothing of the velocity data, and respiratory gating would be useful to increase the data quality in future studies. No respiratory motion induced ghosting artifacts were seen in the acquired velocity data, however. The relatively low temporal resolution of these data may result in an underestimation of the pressure gradient field. This will smooth the relative pressure in the temporal dimension, as discussed by Yang et al. [12]. However, comparison of the MRI-derived data with velocity data obtained from Doppler continuous wave ultrasound, which has a sampling frequency of 250 Hz, indicates that this effect is small [10]. The spatial resolution is also limited, and may be insufficient for calculation of the second derivatives necessary for the viscous resistance. The effect of viscous resistance on the pressure field is expected to be negligible, however. The small amount of noise present in the velocity data is not expected to influence the obtained pressure field significantly, as the calculated pressure field is, in principle, a least-square solution. It may be reflected in a slower convergence of the Poisson solver. In this study, the PPE is solved using the Jacobi iteration method, which was chosen mainly for its simplicity and general applicability. Its major shortcoming is its slow convergence, which is true for most other relaxation methods as well. More specialized methods, such as a multigrid [37] or a direct FFT-based method [38], may be more efficient.

Conclusion

Three-dimensional *in vivo* velocity and relative pressure fields reveal new insights into normal human cardiac pressure dynamics. The ability to noninvasively measure and visualize these three-dimensional velocity and relative pressure fields provides a promising tool for future studies of cardiac function and flow, and for refinement of numerical simulations. They offer an opportunity to expand our understanding of the basic determinants of time-varying flow in healthy and sick hearts, with the potential for improving our methods for diagnosis, medical treatment, and surgical correction of cardiovascular disease.

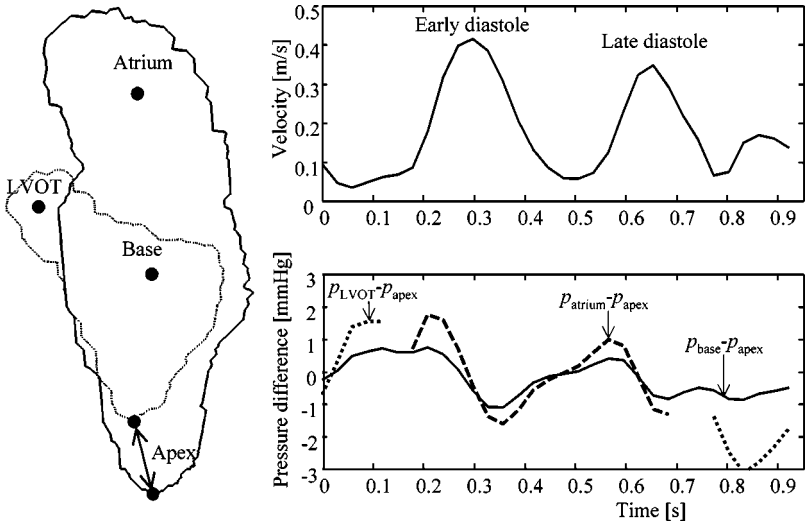

Fig. 5 The velocity at the base and the pressure difference between the left atrium and apex (solid), the base and the apex (dashed), and the left ventricular outflow tract (LVOT) and the apex (dotted) over the cardiac cycle of the healthy volunteer. In the left panel, the localization of the manually placed points is shown in relation to a contour of the blood pool at mid-diastole (solid) and late systole (dotted).

Acknowledgments

This work was supported by the multidisciplinary research school Forum Scientum and the Swedish Foundation for Strategic Research, the Swedish Medical Research Council (K2001-1X-09481-11B), the Swedish Research Council (299-2000-570), the Swedish Heart and Lung foundation (2000-41688, and 2000-41454), and the Center for Industrial Information Technology at Linköping University (99.11).

References

[1] Thomas, J. D., and Weyman, A. E., 1992, ''Numerical Modeling of Ventricular Filling,'' Ann. Biomed. Eng., **20**, pp. 19–39.
[2] Taylor, T. W., and Yamaguchi, T., 1995, ''Flow Patterns in Three-Dimensional Left Ventricular Systolic and Diastolic Flows Determined From Computational Fluid Dynamics,'' Biorheology, **32**, pp. 61–71.
[3] Peskin, C. S., and McQueen, D. M., 1992, ''Cardiac Fluid Dynamics,'' Crit. Rev. Biomed. Eng., **20**, pp. 451–459.
[4] Durand, E. P., Jolivet, O., Itti, E., Tasu, J. P., and Bittoun, J., 2001, ''Precision of Magnetic Resonance Velocity and Acceleration Measurements: Theoretical Issues and Phantom Experiments,'' J. Magn. Reson Imaging, **13**, pp. 445–451.
[5] Lingamneni, A., Hardy, P., Powell, K., Pelc, N., and White, R., 1995, ''Validation of Cine Phase-Contrast MR Imaging for Motion Analysis,'' J. Magn. Reson Imaging, **5**, pp. 331–338.
[6] Nordell, B., Ståhlberg, F., Ericsson, A., and Ranta, C., 1988, ''A Rotating Phantom for the Study of Flow Effects in MR Imaging,'' Magn. Reson. Imaging, **6**, pp. 695–705.
[7] Kim, W. Y., Walker, P. G., Pedersen, E. M., Poulsen, J. K., Oyre, S., Houlind, K., and Yoganathan, A. P., 1995, ''Left Ventricular Blood Flow Patterns in Normal Subjects: A Quantitative Analysis by Three-Dimensional Magnetic Resonance Velocity Mapping,'' J. Am. Coll. Cardiol., **26**, pp. 224–238.
[8] Fyrenius, A., Wigström, L., Bolger, A. F., Ebbers, T., Öhman, K. P., Karlsson, M., Wranne, B., and Engvall, J., 1999, ''Pitfalls in Doppler Evaluation of Diastolic Function: Insights From Three-Dimensional Magnetic Resonance Imaging,'' J. Am. Soc. Echocardiogr, **12**, pp. 817–826.
[9] Fyrenius, A., Wigström, L., Ebbers, T., Karlsson, M., Engvall, J., and Bolger, A. F., 2001, ''Three Dimensional Flow in the Human Left Atrium,'' Heart, **86**, pp. 448–455.
[10] Ebbers, T., Wigström, L., Bolger, A. F., Engvall, J., and Karlsson, M., 2001, ''Estimation of Relative Cardiovascular Pressures Using Time-Resolved Three-Dimensional Phase Contrast MRI,'' Magn. Reson. Med., **45**, pp. 872–879.
[11] Song, S. M., Leahy, R. M., Boyd, D. P., Brundage, B. H., and Napel, S., 1994, ''Determining Cardiac Velocity Fields and Intraventricular Pressure Distribution From a Sequence of Ultrafast CT Cardiac Images,'' IEEE Trans. Med. Imaging, **13**, pp. 386–397.
[12] Yang, G. Z., Kilner, P. J., Wood, N. B., Underwood, S. R., and Firmin, D. N., 1996, ''Computation of Flow Pressure Fields From Magnetic Resonance Velocity Mapping,'' Magn. Reson. Med., **36**, pp. 520–526.
[13] Tyszka, J. M., Laidlaw, D. H., Asa, J. W., and Silverman, J. M., 2000, ''Three-Dimensional, Time-Resolved (4D) Relative Pressure Mapping Using Magnetic Resonance Imaging,'' J. Magn. Reson Imaging, **12**, pp. 321–329.
[14] Wigström, L., Ebbers, T., Fyrenius, A., Karlsson, M., Engvall, J., Wranne, B., and Bolger, A. F., 1999, ''Particle Trace Visualization of Intracardiac Flow Using Time Resolved 3D Phase Contrast MRI,'' Magn. Reson. Med., **41**, pp. 793–799.
[15] Wigström, L., Sjöqvist, L., and Wranne, B., 1996, ''Temporally Resolved 3D Phase-Contrast Imaging,'' Magn. Reson. Med., **36**, pp. 800–803.
[16] Knutsson, H., and Westin, C. F., 1993, ''Normalized and Differential Convolution: Methods for Interpolation and Filtering of Incomplete and Uncertain Data,'' presented at IEEE Computer Society Conference on Computer Vision and Pattern Recognition, New York.
[17] Irarrazabal, P., and Nishimura, D. G., 1995, ''Fast Three Dimensional Magnetic Resonance Imaging,'' Magn. Reson. Med., **33**, pp. 656–662.
[18] Madore, B., Fredrickson, J. O., Alley, M. T., and Pelc, N. J., 2000, ''A Reduced Field-of-View Method to Increase Temporal Resolution or Reduce Scan Time in Cine MRI,'' Magn. Reson. Med., **43**, pp. 549–558.
[19] Bernstein, M., Zhou, X., Polzin, J., King, K., Ganin, A., Pelc, N., and Glover, G., 1998, ''Concomitant Gradient Terms in Phase Contrast MR: Analysis and Correction,'' Magn. Reson. Med., **39**, pp. 300–308.
[20] Pelc, N. J., Sommer, F. G., Li, K. C., Brosnan, T. J., Herfkens, R. J., and Enzmann, D. R., 1994, ''Quantitative Magnetic Resonance Flow Imaging,'' Magn. Reson. Q., **10**, pp. 125–147.
[21] Panton, R. L., 1984, *Incompressible flow*, John Wiley and Sons, New York.
[22] Anderson, D. A., Tannehill, J. C., and Pletcher, R. H., 1984, *Computational Fluid Mechanics and Heat Transfer*, Hemisphere, Washington DC.
[23] Gresho, P. M., and Sani, R. L., 1987, ''On Pressure Boundary Conditions for the Incompressible Navier-Stokes Equations,'' Int. J. Numer. Methods Fluids, **7**, pp. 1111–1145.
[24] Anderson, J. D., 1995, *Computational Fluid Dynamics*, McGraw-Hill, New York.
[25] Golub, G. H., and Van Loan, C. F., 1996, *Matrix Computations*, The John Hopkins University Press, Baltimore, MD.
[26] Sarnoff, S. J., Gilmore, J. P., and Mitchel, J. H., 1962, ''Influence of Atrial Contraction and Relaxation on Closure of Mitral Valve. Observations on Effect of Autonomic Nerve Activity,'' Circ. Res., **11**, pp. 26–35.
[27] Noble, M. I., 1968, ''The Contribution of Blood Momentum to Left Ventricular Ejection in the Dog,'' Circ. Res., **23**, pp. 663–670.
[28] Falsetti, H. L., Verani, M. S., Chen, C. J., and Cramer, J. A., 1980, ''Regional Pressure Differences in the Left Ventricle,'' Cathet. Cardiovasc. Diagn., **6**, pp. 123–134.
[29] Courtois, M., Kovács, Jr., S. J., and Ludbrook, P. A., 1988, ''Transmitral Pressure-Flow Velocity Relation; Importance of Regional Pressure Gradients in the Left Ventricle During Diastole,'' Circulation, **78**, pp. 661–671.
[30] Courtois, M., Kovács, Jr., S. J., and Ludbrook, P. A., 1990, ''Physiological Early Diastolic Intraventricular Pressure Gradient is Lost During Acute Myocardial Ischemia,'' Circulation, **81**, pp. 1688–1696.
[31] Nikolic, S. D., Feneley, M. P., Pajaro, O. E., Rankin, J. S., and Yellin, E. L., 1995, ''Origin of Regional Pressure Gradients in the Left Ventricle During Early Diastole,'' Am. J. Physiol., **268**, pp. H550–H557.
[32] Smiseth, O. A., Steine, K., Sandbæk, G., Stugaard, M., and Gjølberg, T., 1998, ''Mechanics of Intraventricular Filling: Study of LV Early Diastolic Pressure Gradients and Flow Velocities,'' Am. J. Physiol., **275**, pp. H1062–H1069.
[33] Bellhouse, B. J., and Bellhouse, F. H., 1969, ''Fluid Mechanics of the Mitral Valve,'' Nature (London), **224**, pp. 615–616.
[34] Reul, H., Talukder, N., and Müller, E. W., 1981, ''Fluid Mechanics of the Natural Mitral Valve,'' J. Biomech., **14**, pp. 361–372.
[35] Yellin, E. L., Peskin, C., Yoran, C., Koenigsberg, M., Matsumoto, M., Laniado, S., McQueen, D., Shore, D., and Frater, R. W., 1981, ''Mechanisms of Mitral Valve Motion During Diastole,'' Am. J. Physiol., **241**, pp. H389–H400.
[36] Ebbers, T., 2001, ''Cardiovascular Fluid Dynamics—Methods for Flow and Pressure Field Analysis From Magnetic Resonance Imaging,'' Linköping Studies in Science and Technology Dissertations, No. 690, Linköping University, Linköping, Sweden.
[37] Averbuch, A., Israeli, M., and Vozovoi, L., 1998, ''A Fast Poisson Solver of Arbitrary Order Accuracy in Rectangular Regions,'' SIAM J. Sci. Comput. (USA), **19**, pp. 933–952.
[38] Kuo, C.-C. J., and Levy, B. C., 1990, ''Discretization and Solution of Elliptic PDEs—A Digital Signal Processing Approach,'' Proc. IEEE, **78**, pp. 1808–1842.